Geophysical Research Letters

RESEARCH LETTER
10.1029/2021GL094109

Stratigraphic Evidence for Early Martian Explosive Volcanism in Arabia Terra

Patrick Whelley[1], Alexandra Matiella Novak[2], Jacob Richardson[1], Jacob Bleacher[3], Kelsey Mach[4], and Reagan N. Smith[5]

[1]University of Maryland, College Park, MD, USA, [2]Applied Physics Laboratory, Johns Hopkins University, Laurel, MD, USA, [3]NASA-Goddard Space Flight Center, Greenbelt, MD, USA, [4]Landau Associates, Inc., Seattle, WA, USA, [5]Pennsylvania State University, State College, PA, USA

Key Points:

- Layered deposits are found at seven locations in Arabia Terra involving minerals consistent with or diagnostic of altered volcanic ash
- Volcanic ash deposits documented here thin away from previously suggested sources, consistent with supereruption model predictions
- Between 1 and 2 thousand caldera-forming eruptions over 500 million years from western Arabia Terra are needed to produce the observed ash

Supporting Information:

Supporting Information may be found in the online version of this article.

Correspondence to:

P. Whelley,
patrick.l.whelley@nasa.gov

Citation:

Whelley, P., Matiella Novak, A., Richardson, J., Bleacher, J., Mach, K., & Smith, R. N. (2021). Stratigraphic evidence for early martian explosive volcanism in Arabia Terra. *Geophysical Research Letters*, *48*, e2021GL094109. https://doi.org/10.1029/2021GL094109

Received 29 APR 2021
Accepted 12 JUL 2021

Abstract Several large paterae in Arabia Terra are suggested to be calderas that produced colossal explosive eruptions (i.e., supereruptions). If these features are indeed explosive calderas, dispersion modeling suggests extensive ash deposits should be common throughout the region. However, such deposits have not previously been linked with the suggested calderas. Here, we describe layered deposits containing minerals both consistent with and diagnostic of altered volcanic ash throughout Arabia Terra. These deposits include Al-dominant minerals such as montmorillonite, imogolite, and allophane among others. Altered ash deposits are found to thin (from 1-km to 100-m thickness) away from the suggested calderas. We estimate that the volcanic ash observed in Arabia Terra is the result of between 1,000 and 2,000 individual explosive eruptions over 500-million years. Our observations support the hypothesis that Arabia Terra hosted supereruptions in the late Noachian-early Hesperian that repeatedly blanketed the region with layers of ash.

Plain Language Summary Several large and deep craters in western Arabia Terra, Mars are thought to be explosive calderas, a type of volcano capable of producing supereruptions. If these craters are calderas, vast layers of volcanic ash should be common in Arabia Terra. While layered deposits have been observed previously in Arabia, until now, no deposits have been associated with the suggested calderas. We present mineral signatures of volcanic ash deposits that thin (from 1 km to 100 m thickness) away from the suggested calderas. Our observations support the idea that explosive calderas do exist in western Arabia Terra, and they produced thousands of super eruptions spread out over 500 million years of ancient Mars history.

1. Introduction

1.1. Martian Volcanism and Missing Vents

Volcanism is a fundamental process involved in nearly every aspect of Mars' evolution (Greeley & Schneid, 1991; Greeley & Spudis, 1981; Zuber, 2001) throughout the planet's history (Brož et al., 2021; Carr, 1973; Hodges & Moore, 1994; Richardson, Bleacher et al., 2021). Magma production through time and the intimately linked contribution of volcanic gases to the atmosphere are inferred by several approaches (Craddock & Greeley, 2009; Crown & Greeley, 1993; Gaillard et al., 2013; Gillmann et al, 2011; Greeley, 1987; Greeley & Schneid, 1991; Lammer et al., 2013; Phillips et al., 2001; Plescia & Crisp, 1992). Although estimates disagree in detail, all models suggest that an early (Noachian–Hesperian) high magma production rate tailed-off to limited or no production at present (e.g., Horvath et al., 2021). Despite extensive evidence of volcanic activity across ancient Mars, only ~75 ancient volcanic edifices have been identified or proposed (Crown & Greeley, 1993; Greeley & Crown, 1990; Williams et al., 2009; Xiao et al., 2012). Much of the ancient martian crust has been resurfaced by volcanic materials from unidentified sources (Golombek et al., 2006). It is unclear if Noachian–Hesperian volcanoes remain under-identified because (a) evidence for them has been buried or eroded away (Golombek et al., 2006; Xiao et al., 2012), (b) evidence has until recently been overlooked due to limits in data resolution and coverage, or (c) some ancient explosive volcanoes (e.g., Peneus, Malea, and Pityusa Paterae [Williams et al., 2009]) are fundamentally different than those associated with well-characterized edifice-forming volcanoes and therefore remain unrecognized.

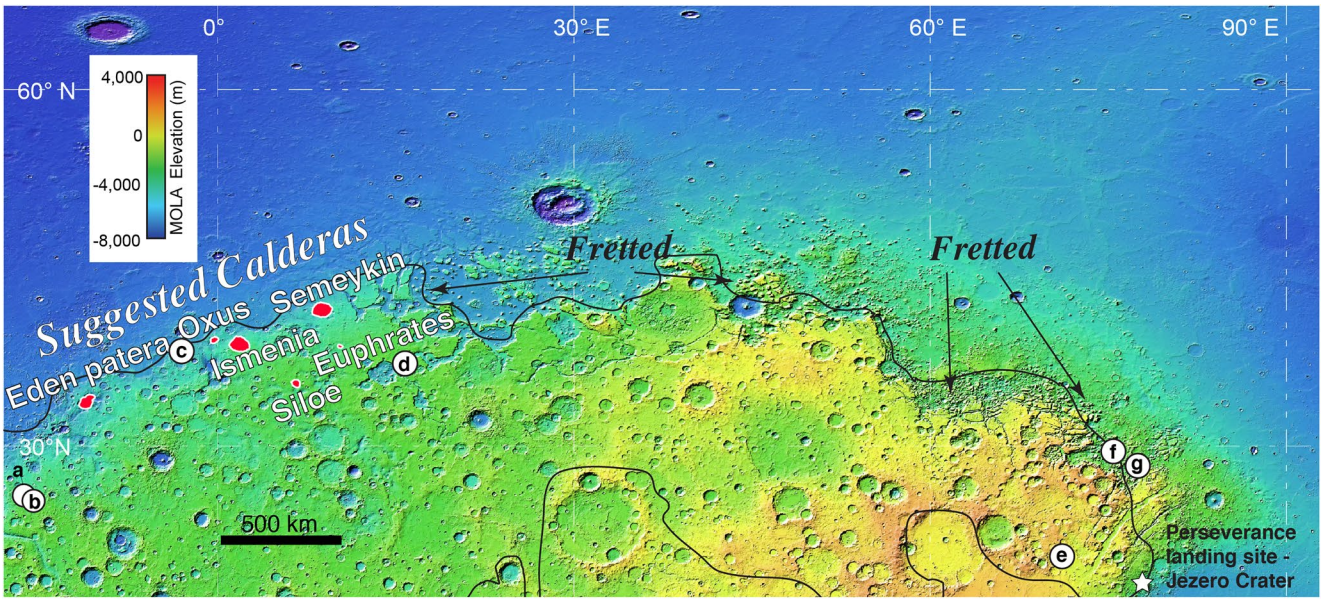

Figure 1. Arabia Terra and the Fretted Terrain. Red polygons mark the locations of the suggested calderas while the white circles a–g correspond to observations of altered volcanic ash and indicate locations of interest discussed in this paper. The Perseverance Rover landing site is noted with a white star. The base map is topographic shaded-relief derived from Mars Orbiter Laser Altimeter gridded data.

1.2. Arabia Terra & Fretted Terrain

Volcanic deposits have been suggested to exist in Arabia Terra (e.g., Moore, 1990) although few vents are identified in the region (Brož et al., 2021). Fretted terrain comprises much of the northern boundary of this region and is defined as smooth low-lying plains separated from complex plateaus by cliffs (Sharp, 1973) forming a polygonal network of canyons (Figure 1). The fretted terrain unit is composed of altered, fine-grained, layered, clay- and sulphate-bearing sediments suggested to be eroded ancient explosive volcanic deposits (e.g., Fassett & Head, 2007; Hynek et al., 2003; Moore, 1990). Given its regional extent, spanning >2,500-km, a volcanic provenance of the unit would be indicative of voluminous explosive volcanism. However, this explanation remains unconfirmed because it has two important deficiencies: (a) logical source(s) (Kerber et al., 2012) and (b) direct evidence of volcanic deposits.

Mapping of Arabia Terra indicates that the region experienced volcanic activity (McGill, 2000). Michalski and Bleacher (2013) suggest that seven large depressions in the region represent old explosive volcanic centers analogous to the Circum-Hellas paterae (Williams et al., 2009). The features are characterized by large collapse structures with low or no rim topographic relief, and associations with ridged lava plains. They referred to the features as "plains-style caldera complexes," but here we refer to them as "suggested calderas." Michalski and Bleacher (2013) present evidence for large calculated erupted volumes, collapse, low relief, and resurgent domes consistent with terrestrial explosive calderas. If these features are indeed explosive calderas, ash dispersion modeling (e.g., Glaze and Baloga, 2002; Kerber et al., 2012; Keber, Forget et al., 2013; Keber, Michalski et al., 2013) suggests extensive ash deposits, carried by ancient winds, should be common throughout Arabia Terra. The kilometer-deep canyon walls within the fretted terrain should therefore expose evidence for Noachian-Hesperian era volcanic deposits.

Here, we present observations that support the hypothesis that Arabia Terra was the site of early martian supereruptions (i.e., explosively erupted volumes ≥1,000 km^3) which produced regionally blanketing pyroclastic deposits. We describe seven individual observations (Figure 1) of layered deposits exposed in cliff faces and a detailed study of their mineralogy using CRISM (Compact Reconnaissance Imaging Spectrometer for Mars) data (Murchie et al., 2007), and morphology using HiRISE (High Resolution Imaging Science Experiment; [McEwen et al., 2007]) and CTX (Context Camera) data (Malin et al., 2007).

2. Methodology

2.1. Identifying Mineralogical Signatures of Volcanic Ash

A survey of CRISM images of cliff faces and crater walls in Arabia Terra was conducted to identify mineralogical signatures of volcanic ash. CRISM is well suited for this task because the alteration of volcanic ash deposits leads to unique mineral assemblages that can be readily distinguished with spectral remote sensing. For example, hydrated silica, zeolites, clays and sulfates could all be products of altered volcanic ash detected visible/near-infrared (VNIR) and short-wave infrared (SWIR) instrumentation such as CRISM (Liu et al., 2021; Murchie et al., 2007; Rampe et al., 2012; K. D. Seelos et al., 2010; Viviano-Beck et al., 2014; Ye & Michalski, 2021). K. D. Seelos et al. (2010) analyzed Airborne Visible/Near-Infrared Imaging Spectrometer (AVIRIS) data over Kilauea Volcano, Hawaii, and found that the ash spectral endmember is characterized by VNIR features suggestive of poorly crystalline iron oxides, while SWIR features at 2.25-μm indicate the presence of opaline silica. Zeolites can form where volcanic rock and ash layers react with alkaline groundwater (Eugster, 1980; Sheppard & Hay, 2001; Weisenberger & Selbekk, 2009). Additional field studies at Kilauea Volcano further constrained minerals assemblage associated with the weathering of volcanic ash and basalt, including Fe/Mg smectite and opaline silica, which occur in relatively arid and acidic environments (Schiffman et al., 2006; Sherman & Uehara, 1956). Terrestrial analog studies have also found montmorillonite associated with hydrothermal alteration of impact structures (e.g., Osinski, 2005; Svenson et al, 2021), but the most common origin, when the deposits are layered is altered volcanic ash (Clark et al., 2007; Ehlmann et al., 2013).

We utilized CRISM Map Projected Targeted Reduced Data Record (MTRDR) products to analyze the mineralogy. MTRDRs are derived from CRISM hyperspectral targeted observations processed through a series of standard and empirical spectral corrections, spatial transforms, summary parameter calculations, atmospheric corrections, and renderings (F. P. Seelos et al., 2012). Hyperspectral images analyzed include full-resolution targeted (FRT) images (~20-m/pixel resolution) and half-resolution long (HRL) targeted image (~40-m/pixel resolution). Each CRISM image described here was analyzed using ENVI-enabled spectral interpretation tools (following methods of Viviano-Beck et al. [2017] and Buczkowski et al. [2020]) to collect spectral signatures of mineralogy assemblages that are indicative of altered volcanic ash. Spectra were ratioed for an area covering spectrally neutral material within the same detector column, to accentuate weak spectral features and remove any residual column-dependent noise. Locations suggested in CRISM images to contain volcanic ash (i.e., locations of interest) were followed-up with morphologic and morphometric analysis using topographic data.

2.2. Morphologic and Morphometric Analysis

Digital Elevation Models (DEMs) of locations of interest (identified through CRISM analysis to have volcanic ash) within the Arabia Terra study area were produced from high-resolution images from the Context Imager (CTX) aboard the Mars Reconnaissance Orbiter, using the Ames Stereo Pipeline (ASP) (Moratto et al., 2010). Images were selected to overlap CRISM targets of interest to produce co-located geomorphologic and mineralogic observations. The DEMs were processed using two CTX images that are spatially overlapping, that is, are stereopairs. Stereopairs with adequately matching illumination and sufficient convergence angles at locations of interest were identified using the Planetary Image Locator Tool (PILOT) (Bailen et al., 2015) and suggested complementary attributes as detailed by Becker et al. (2015) and Bailen et al. (2015). For each location of interest, both stereo images were downloaded from the PDS. Additional HiRISE DEMs in the study area which are publicly available from the HiRISE website (https://hirise.lpl.arizona.edu/) were also downloaded for this project. DEMs were constructed using the photogrammetric toolkit ASP. Processed CTX DEMs were aligned to Precision Experiment Data Records (PEDRs) from the Mars Orbiter Laser Altimeter (MOLA [Smith et al., 2001]) to reference the DEM to the martian aeroid. All DEMs were exported in a Mars sinusoidal coordinate system for GIS ingestion.

Both topographic and mineralogic imaging data were imported into GIS software where the co-registration between each CTX DEM and CRISM cube was manually validated. CRISM images were draped over the

DEMs (following Viviano-Beck et al. [2017]), to produce a three-dimensional visualization of the vertical topography and enable quantitative measurements (e.g., thickness and slope) of layering within observed mineralogic units. Topographic profiles were analyzed across mineral contacts and over steep terrain to aid visualization and used to measure layer thickness (Figure 2). We corrected for apparent dips by measuring layer attitudes in the DEMs to extract best estimates of layer thicknesses.

3. Results

Morphologically coherent and mineralogically distinct layers were found at seven locations of interest (Figure 1, ESM) where we produced DEMs (J. A. Richardson, Whelley et al., 2021) and scrutinized CRISM spectra. Combining CRISM data with CTX DEMs in steep topography (e.g., cliff faces and crater walls) confirmed that spectral signatures of different mineral species were found to exist in vertically separated coherent layers with low dip, as is expected of volcanic ash fall deposits. We found both altered and unaltered minerals. Unaltered minerals found include olivine and pyroxene, but these could just as likely originate from lava flows and are not diagnostic of explosive deposits. Therefore, we focused on mineralogical species commonly associated with altered volcanic ash that were present (Figure 2). For clarity, we separate observed species into (a) minerals that are consistent with volcanic ash but could also have had non-volcanic origins (Milliken et al., 2008; Murchie et al., 2007; Perrin et al., 2019; Schiffman et al., 2006; K. D. Seelos et al., 2010; Sherman & Uehara, 1956; Viviano-Beck et al., 2014) and (b) minerals that are diagnostic of volcanic ash (Bishop et al., 2013; Bishop & Rampe, 2016; Hewett & Lupton, 1917; Keller, 1970; Liu et al., 2021; McKeown et al., 2009; Ross & Shannon, 1926; Wherry, 1917; Ye & Michalski, 2021).

Minerals consistent with ash include hydrated sulfates (e.g., jarosite), phyllosilicates (e.g., Mg and Fe smectites) and hydrated silicas (opals). Observed minerals that are diagnostic of altered volcanic ash include Al-phyllosilicates (e.g., Al smectites–such as montmorillonite–imogolite, and allophane; e.g., McKeown et al, 2009 and Bishop et al., 2013). Al-phyllosilicates are particularly prevalent around Mawrth Vallis and the greater Arabia Terra Region (Viviano-Beck, et al., 2014). The studies cited in the previous paragraph focus on climatic conditions on Mars that would be needed to alter various materials into the diversity of minerals observed today. Results presented here build upon these interpretations to further characterize the distribution and thickness of altered minerals as an indicator of past volcanic activity.

We present results for Western and Eastern Arabia separately; dust cover in central Arabia Terra (Ruff & Christensen, 2002) inhibited clear CRISM bedrock observations, which complicated obtaining clear spectral signatures from orbital data.

3.1. Western Arabia

Locations of interest a through d (Figure 1) span locations in western Arabia where the spectral data reveal both clear, well-defined layers (e.g., a) and mineral mixing (e.g., b). Location a includes two adjacent craters with exposed layering (Figure 2). Locations a and b are within the Mawrth Vallis region. In these two locations of interest as well as in another in western Arabia (c), spectrally dominant mineral species include Fe- and Mg-smectites (nontronite and saponite) Al-smectite (montmorillonite), aluminosilicates (allophane, imogolite), hydrated silica (opal), and infrequently hydroxylated sulphate (jarosite) are mixed in with Fe/Mg smectites and hydrated silica. The presence of montmorillonite, allophane, and imogolite, in particular, are diagnostic of the alteration of volcanic ash fall deposits. The presence of nontronite has also been chemically linked to the deposition of a fresh volcanic ash layer in a cold, limited-water environment (Bishop et al., 2020).

At location (a), we observe a unit in the crater rim that is a mix of imogolite, allophane and some jarosite, with weak absorption features at 1.85 and 2.26-μm (indicative of jarosite) and stronger absorptions at 1.92 and 2.2-μm. Stratigraphically below that, in the upper part of the crater wall, is a layer of montmorillonite and hydrated silica, with absorption features at 1.41, 1.91 and 2.21-μm. A middle crater wall unit is spectrally dominated by Fe/Mg smectites having absorption features at 1.41–1.42-μm, 1.91-μm, and at a variable wavelength center from 2.28 to 2.32-μm. Also present in this unit is a strong absorption feature at 1.94 μm

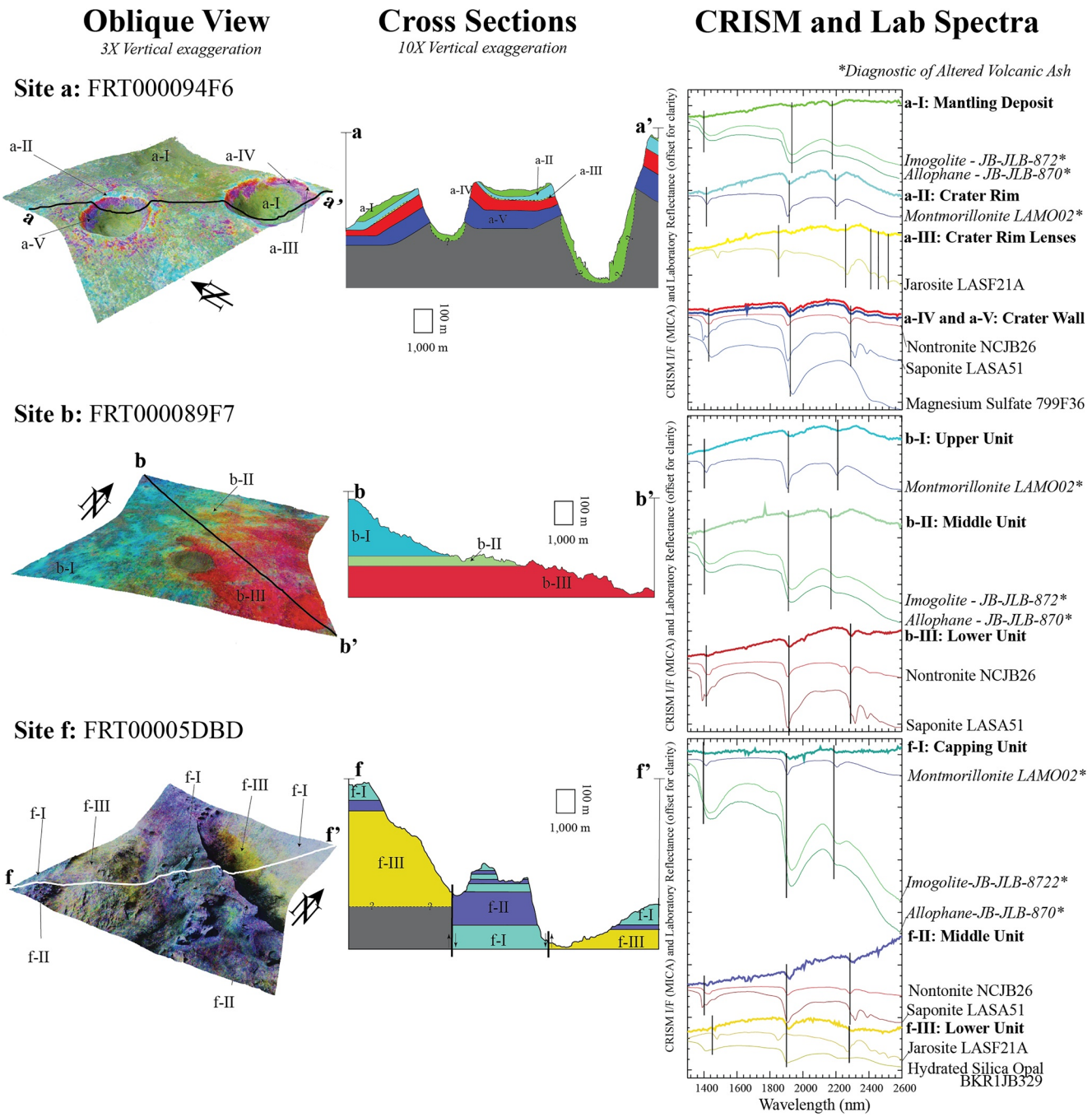

Figure 2. Oblique views of Compact Reconnaissance Imaging Spectrometer for Mars (CRISM) images at locations of interest a, b, and f (left), over Context Camera (CTX) topography and shading. Interpreted cross sections (center) are based on the mineralogy observed in CRISM and co-located CTX topography. (right) CRISM spectra (bold lines) compared to lab spectra (thin lines) for locations of interest a, b, and f. Mineral names in italics are diagnostic of volcanic ash while all others are consistent with ash. The colors are from CRISM parameters (Red = bd2265, Green = bd2250, Blue = sindex2) as defined by Viviano-Beck et al. (2014). The reddish areas are spectrally dominated by Fe/Mg smectite, the light bluish areas by Al-phyllosilicates, such as montmorillonite, and the greenish areas by aluminosilicates such as allophane and imogolite. Yellow areas are spectrally dominated by jarosite.

which could indicate the presence of Mg-dominated polyhydrated sulfates. Within the topographic profile at location (a) (Figure 2) the thickness of material diagnostic of altered volcanic ash total ~190-m and that consistent with volcanic ash include an additional 10 m. This sums to a possible 200-m of altered volcanic ash.

Approximately 25-km to the southeast, CRISM images for location b show three distinct layers. The upper layer has absorption features centered at 2.2-μm, suggesting the presence of Al-smectite (montmorillonite). The middle layer has strong allophane/imogolite signatures with absorption features at 1.39–1.40, 1.92, and 2.19–2.20-μm. The lower layer displays absorption features at 1.91, 1.42, and 2.3-μm indicating the presence of Fe/Mg smectite. Some jarosite might also be present as a smectite-jarosite mix, as suggested by a feature whose center varies spatially from 2.29 to 2.26-μm. Together the montmorillonite, allophane/imogolite package, minerals diagnostic of volcanic ash, are about 290-m thick within location (b).

At location (c), within a central crater pit of a crater approximately 52-km in diameter, CRISM observations show similar mineral assemblages as in other regions of Western Arabia Terra. Units dominated by diagnostic minerals such as montmorillonite, and mixed with imogolite and allophane, are observed in layers alternating vertically with layers dominated by Fe/Mg smectite mixed with jarosite. Diagnostic material at location **c** total ~800-m in thickness, whereas material consistent with altered volcanic ash is about 200-m, forming a combined stratigraphic package ~1000-m thick. Location (c) is the closest site to the paterae identified by Michalski and Bleacher (2013) and represents the maximum thickness of altered ash units observed in CRISM images in the study.

CRISM observations at location (d) show layered material consistent with other observations in this study. Layers dominated spectrally by Fe/Mg smectites are interlayered with layers spectrally dominated by montmorillonite, allophane and imogolite. There are also some instances of jarosite mixed in with both the Fe/Mg smectites and the Al-dominated units (imogolite, allophane and montmorillonite) that are diagnostic of altered volcanic ash. Units diagnostic of altered volcanic ash at location (d) total~ 550-m thick and units consistent with altered volcanic ash are about 150-m thick, for a combined thickness of ~700-m.

3.2. Eastern Arabia

In the eastern portion of the study area (e, f, g), near the Nili Fossae region, CRISM observations show finer scale (<10-m) interlayered sequences of potentially altered volcanic ash units. A plateau unit in f displays alternating layers of montmorillonite, mixed with imogolite and allophane, and Fe/Mg smectites (Figure 2). On either side of the plateau, weaker absorption features detected by CRISM show a more massive unit that is spectrally dominated by hydrated silica mixed with jarosite and Fe/Mg smectites. At site f, layers that are consistent with altered volcanic ash are ~400-m thick and layers diagnostic of altered volcanic ash are ~100-m thick, for a total thickness of ~500-m.

To the southeast (g), these same minerals exist, also in thinner alternating layers than in western Arabia Terra. At this site, Fe/Mg smectite is exposed in lower units within the CRISM scene. Material consistent with altered volcanic ash are ~50-m thick and layers diagnostic of altered volcanic ash are ~600-m thick for a total thickness of about 650-m. However, the bulk of the deposits make up the rim of an impact crater and are therefore potentially overthickened by impact processes.

Further south (e), CRISM data reveal abundant Fe/Mg smectite, sporadically mixed with jarosite, in stratigraphically higher units. Layers rich in montmorillonite, imogolite and allophone dominate lower units. As with the other sites in eastern Arabia Terra, these layers are thinner with more frequent alternating sequences of mineral assemblages than in Western Arabia Terra. At location **e**, minerals consistent with altered volcanic ash are ~200-m thick and minerals diagnostic of altered volcanic ash are ~100-m thick, for a total thickness of about 300-m.

The mineralogy observed at all locations of interest (a–g) are consistent with previous documentation of spectral signatures in Arabia Terra (Bishop & Rampe, 2016; Gross et al., 2017; Lowe et al., 2020). Particularly relevant are analog studies comparing spectra from Mawrth Vallis with spectra from the Painted Desert in Arizona, that have found jarosite, phyllosilicate, and hydrated silica mixes (e.g., Perrin et al., 2019), which formed from lacustrine and fluvial alteration of volcanic ash. In the following sections we describe the additional step of relating our observations geographically to explore regional trends and provide further insights into the possibility of supereruptions on Mars.

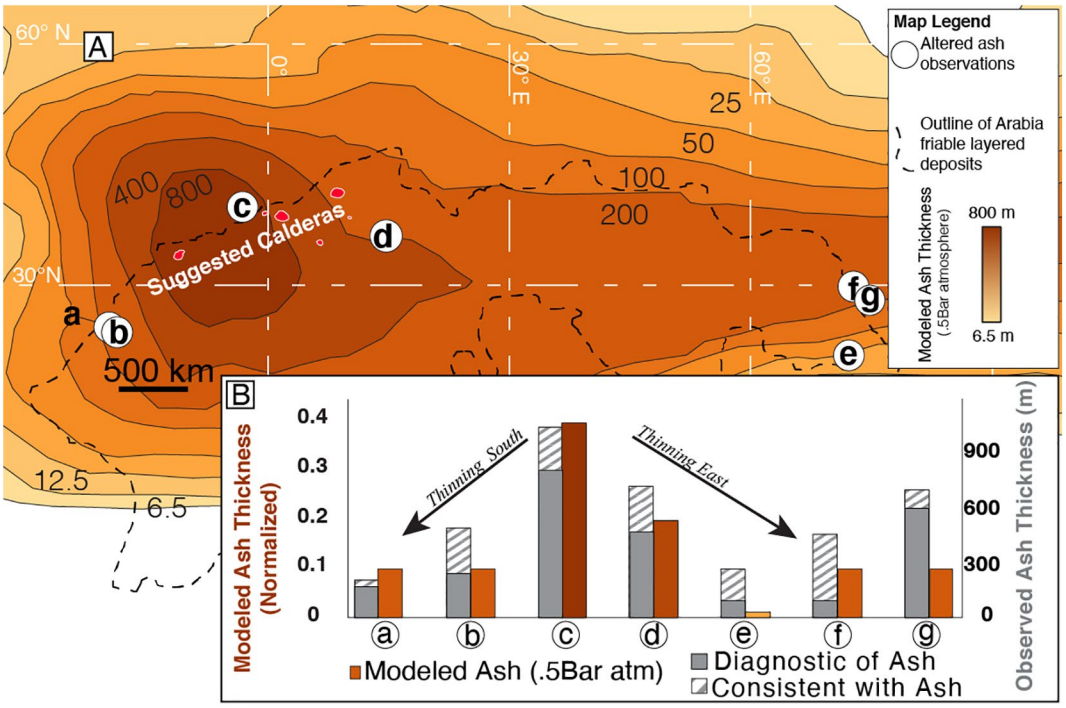

Figure 3. Modeled 35-μm diameter ash deposit thickness (shades of amber [after Kerber, Michalski et al., 2013]) from hypothetical supereruptions from the suggested calderas, into a 0.5-bar atmosphere. (b) compares observed and modeled ash at seven locations of interest. Model results have been normalized to illustrate the regional shape i.e., the thinning to the east (right of the peak) and south (left of peak). Both the model and observations show a systematic decrease in ash thickness with distance from the suggested calderas. The matching model and observation trends (except g, which is anomalously thick) suggest the layered altered ash deposits are linked by a regional process across Arabia Terra.

4. Discussion

4.1. Spatial Distribution

The seven CRISM observations described above are distributed across the study region (Figure 1) and yet, due to substantial dust deposits in central Arabia Terra, are principally located in the eastern and western ends of Arabia Terra. Comparing our observations to ash dispersion models enables us to link these geographically distant observations in a regional narrative.

Previous ash dispersion modeling (Kerber, Michalski et al., 2013) found that if the suggested calderas in western Arabia Terra produced catastrophic eruptions, the ash layers would have been thickest proximal to the calderas, thin to the south and extended to the east thousands of kilometers (Figure 3). It is important to point out that the dispersion modeling was limited to tracking the spread of 5×10^6 km^3 of 35-μm ash and built an annualized distribution by starting a hypothetical eruption each day for one martian year, to avoid a seasonal bias. Real eruptions might have had different deposit shapes depending on many factors.

As a first order comparison of identified altered deposits and potential ash distribution from western Arabia calderas, we normalize (by linear scaling) the Kerber, Michalski et al. (2013) modeled ash thicknesses across the region (Figure 3b). Our ash observations overlap with regions Kerber, Michalski et al. (2013) predicted would have thick (>10s-of-meters) volcanic ash deposits from the suggested calderas. Furthermore, the observed layered deposits in this study are consistent with the distribution pattern found by Kerber, Michalski et al. (2013), with the thickest deposit identified near the potential calderas, and thinning deposits to the south and less rapidly to the east. To further evaluate if the regional trend we are reporting is consistent with catastrophic eruptions from calderas, we turn to terrestrial examples.

4.2. Comparison to Terrestrial Ash Deposits

On Earth, calderas are associated with both effusive (e.g., Mauna Loa, Hawaii; Lockwood & Lipman, 1987) and explosive volcanism (e.g., Yellowstone caldera(s), Wyoming; Wicks et al., 2006), and form due to collapse after evacuation of a large magma reservoir (Cole et al., 2005).

Calderas associated with explosive volcanism on Earth can produce more than 10^{12} m^3 of ash in an eruption (Newhall & Self, 1982), vary widely in shape (e.g., Whelley et al., 2015), range in composition from mafic (e.g., Rooyakkers et al., 2020) to felsic, and rarely sit atop a large stratovolcano (Cole et al., 2005). Explosive caldera-forming eruptions often produce thick ash fall deposits on the flanks and for many 1,000's of kilometers beyond (Newhall & Self, 1982). For example, on Earth, ash fall deposits from two of the largest known eruptions, from Toba and Taupo calderas, and can be found 4,000 km from their respective sources (Matthews et al., 2011).

Modeling shows that the thin atmosphere on Mars today would limit ash dispersion distances (Glaze & Baloga, 2002). However, due to a thicker than present-day atmosphere (e.g., 0.5-bar) on ancient Mars, ash fall deposits would have had a wider distribution than for a similar eruption on Earth (e.g., Brož et al., 2021; Glaze & Baloga, 2002; Kerber et al., 2011, 2012; Kerber, Forget et al., 2013; Wilson & Head, 2007). Therefore, in Arabia Terra, ash fall deposits would be expected to be found >1,000 km from source, that is, throughout the region.

4.3. Comparison to Other Explosive Eruptions on Mars

Altered ash deposits identified in this study are widely distributed within Arabia Terra, and exhibit thicknesses of at least 100-m as far away as 3,400-km from the potential caldera sites. Whereas the thickest deposit identified is up to 1-km in thickness at a distance of ≤250-km from the calderas, no obvious central edifice volcanoes are identified in western Arabia. This morphology deviates from other large martian volcanoes that exhibit evidence of explosivity (Brož et al., 2021). At two such volcanoes, Apollinaris and Hadriacus Mons, central edifices were developed that rise 1–5-km above surrounding topography with basaltic summit calderas 60–90-km in diameter and larger edifice diameters of 100–200-km. The lack of similar edifices near the thickest volcanic deposits in Arabia suggests that the eruption style was significantly different than Plinian eruptions that built other martian central volcanoes (Brož et al., 2021). Instead, the broad regional distribution of pyroclasts is consistent with very finely fragmented material. Unlike calderas that are commonly seen at the summits of basaltic central volcanoes, calderas on Earth that form from highly fragmented explosive eruptions generally have negative topographic expressions, like those identified by Michalski and Bleacher (2013). Although it is possible that large Noachian volcanoes that sourced these prodigious ashes have been eroded beyond recognition, (Kerber, Michalski et al, 2013), our study indicates that the source or sources of Arabia Terra ash deposits were likely in western Arabia Terra and therefore could have been the paterae identified by Michalski and Bleacher (2013).

4.4. Implications on the Eruption History of Western Arabia Terra

The observed deposits of altered volcanic material presented here are broadly consistent with the distribution of ash from sources in western Arabia Terra as modeled by Kerber, Michalski et al. (2013), which shows similar trends of thinning deposits with distance from the suggested calderas to the south and east (Figure 3). Our observed deposits of material that are diagnostic of ash are on average 1.5 times thicker than thicknesses produced by the Kerber et al. model at each site investigated. The modeled thicknesses simulated by Kerber et al. were produced using a total eruption volume of 5×10^6 km^3, which is based on the volume of fine material in Arabia reported by Tanaka (2000). Additionally, all observed deposits in this study, including material diagnostic of and consistent with volcanic ash, average three times thicker than the modeled deposits at each site in this study. Although future identification of more related deposits in and surrounding Arabia will better constrain ashfall isopachs in this region, we interpret the thicknesses of observed deposits in this study to represent a total eruptive volume of 7.5×10^6 to 1.5×10^7 km^3 from western Arabia Terra, based on the comparison between thicknesses identified in this study (for material that is diagnostic of ash and for all altered material, respectively) and modeled thicknesses by Kerber, Michalski et al. (2013).

The amount of magma and number of explosive eruptions required to deposit this volume of material over Arabia Terra and beyond can be estimated using the volumes of the suggested calderas as reported by Michalski and Bleacher (2013). The average depression volume for these paterae is >3,300-km^3 (Michalski & Bleacher, 2013). Assuming bulk densities of 1,300-kg/m^3 for tephra and 2,800-kg/m^3 for magma, Michalski and Bleacher estimated "average minimum erupted volumes" of tephra would be 7,200-km^3 per caldera-forming event. To amass the volume of ash represented in the observed deposits in this study ($7.5–15 \times 10^6$ km^3), western Arabia would need 1,000–2,000 caldera forming eruptions between the Mid Noachian and Early Hesperian Periods when Arabia Terra was formed (Michalski & Bleacher, 2013; Platz et al., 2013; Tanaka, 2000). Furthermore, the total erupted volume over this time would have required 3.5×10^6 km^3 of magma at a minimum to account for the material identified here to be diagnostic of altered volcanic ash and a maximum magma volume of 7×10^6 km^3 to account for all possible altered volcanic ash deposits. As a comparison, these volumes of magma are 30%–60% of the total volume of Olympus Mons (Isherwood et al., 2013). If, during the 500 Ma encompassing the mid-Noachian to early Hesperian epochs, the number of active source regions remained constant and is now represented by the paterae identified by Michalski and Bleacher, these 1,000–2,000 eruptions would have been sourced from seven central volcanoes each with an average repose interval of 1.8–3.5-million years between eruptions.

5. Conclusions

Through a combination of hyperspectral and topographic analyses, we have identified the presence altered volcanic ash layers in Arabia Terra and quantified their thicknesses and distribution. Seven examples of interbedded hydroxy sulfates, smectites, and phyllosilicates that are preserved in distinct layers within the fretted terrain strata suggest that large packages of volcanic ash were produced in Arabia Terra in the late Noachian-early Hesperian periods. In western Arabia Terra, minerals diagnostic of altered volcanic ash observed in CRISM data, including montmorillonite, imogolite and allophane, are distributed in locations consistent with previous observations. The deposits crop out as alternating sequences of minerals that are both consistent with and diagnostic of altered volcanic ash deposits. In eastern Arabia Terra, the same mineral species are found. However, both the mineral packages and the individual mineral layers are thinner than those in the West. The thicknesses of ash layers and their distribution are consistent with ash dispersion modeling (Kerber, Michalski et al., 2013) and with analogous supereruption deposits on Earth. We interpret these findings to suggest that the sources of ash that helped construct Arabia Terra are in western Arabia and could be the calderas identified by Michalski and Bleacher (2013). To deposit the material identified in this study, these sources would have delivered a volume of magma comparable to Olympus Mons to the surface over the late Noachian-early Hesperian periods, potentially generating thousands of large explosive eruptions during their activity.

Data Availability Statement

All stereophotogrammetric DEMs produced for our analysis are currently available on the Digital Repository at the University of Maryland (DRUM) and cited in this manuscript as J. A. Richardson, Whelley et al. (2021; https://drum.lib.umd.edu/handle/1903/27174). CRISM data are available from NASA through the Planetary Data System (PDS) Geoscience Node CRISM archive (https://pds-geosciences.wustl.edu/missions/mro/crism.htm), specific scenes used in this work are indicated in the electronic supplementary material ESM.

Acknowledgments
This work was funded by the Mars Data Analysis Program Grant Number: 80NSSC19K0044. Kelsey Mach was funded through the Goddard Graduate Student Intern Program. Reagan N. Smith was funded through APL's Student Program to Inspire, Relate, and Enrich (ASPIRE). Work by Patrick Whelley and Jacob Richardson was also supported by NASA under award #80GSFC17M0002. The manuscript and figures benefitted from discussions with the Goddard Volcano Writing Group and Christina Viviano, detailed comments from Scott Murchie, and thoughtful reviews by Michalski and an anonymous reviewer; the authors are grateful. Shalom Trudeau.

References

Bailen, M. S., Herkenhoff, K. E., Howington-Kraus, E. A., & Becker, K. J. (2015). Finding Stereo Pairs with the PDS Planetary Image Locator Tool (PILOT). In *46th Lunar and Planetary Science Conference*. pp. 1074. Abstract Retrieved from http://adsabs.harvard.edu/abs/2015LPICo1846.7003B

Becker, K., Archinal, B., Hare, T., Kirk, R., Howington-Kraus, E., Robinson, M., & Rosiek, M. (2015). Criteria for Automated Identification of Stereo Image Pairs. In 46th Lunar and Planetary Science Conference (2015), 1832 (pp. 2703–2704). Retrieved from https://www.hou.usra.edu/meetings/lpsc2015/pdf/2703.pdf

Bishop, J. L., Gross, C., Danielsen, J., Parente, M., Murchie, S. L., Horgan, B., et al. (2020). Multiple mineral horizons in layered outcrops at Mawrth Vallis, Mars, signify changing geochemical environments on early Mars. *Icarus*, *341*, 113634. https://doi.org/10.1016/j.icarus.2020.113634

Bishop, J. L., & Rampe, E. B. (2016). Evidence for a changing Martian climate from the mineralogy at Mawrth Vallis. *Earth and Planetary Science Letters*, *448*, 42–48. https://doi.org/10.1016/j.epsl.2016.04.031
Bishop, J. L., Rampe, E. B., Bish, D. L., Abidin, Z., Baker, L. L., Matsue, N., & Henmi, T. (2013). Spectral and hydration properties of allophane and imogolite. *Clays and Clay Minerals*, *61*(1), 57–74. https://doi.org/10.1346/CCMN.2013.0610105
Brož, P., Bernhardt, H., Conway, S. J., & Parekh, R. (2021). An overview of explosive volcanism on Mars. *Journal of Volcanology and Geothermal Research*, *409*, 107125. https://doi.org/10.1016/j.jvolgeores.2020.107125
Buczkowski, D. L., Seelos, K. D., Viviano, C. E., Murchie, S. L., Seelos, F. P., Malaret, E., & Hash, C. (2020). Anomalous phyllosilicate-bearing outcrops South of Coprates Chasma: A study of possible emplacement mechanisms. *Journal of Geophysical Research: Planets*, *125*, e2019JE006043. https://doi.org/10.1029/2019je006043
Carr, M. H. (1973). Volcanism on Mars. *Reviews of Geophysics and Space Physics*, *78*(20), 4049–4062. https://doi.org/10.1029/jb078i020p04049
Clark, B. C., III, Arvidson, R. E., Gellert, R., Morris, R. V., Ming, D. W., Richter, L., et al. (2007). Evidence for montmorillonite or its compositional equivalent in Columbia Hills, Mars. *Journal of Geophysical Research*, *112*, E06S01. https://doi.org/10.1029/2006JE002756
Cole, J. W., Milner, D. M., & Spinks, K. D. (2005). Carderas and caldera structures: A review. *Earth-Science Reviews*, *69*, 1–26. https://doi.org/10.1016/j.earscirev.2004.06.004
Craddock, R. A., & Greeley, R. (2009). Minimum estimates of the amount and timing of gases released into the martian atmosphere from volcanic eruptions. *Icarus*, *204*(2), 512–526. https://doi.org/10.1016/j.icarus.2009.07.026
Crown, D. A., & Greeley, R. (1993). Volcanic geology of Hadriaca Patera and the Eastern Hellas Region of Mars. *Journal of Geophysical Research*, *98*(E2), 3431–3451. https://doi.org/10.1029/92JE02804
Ehlmann, B. L., Berger, G., Mangold, N., Michalski, J. R., Catling, D. C., Ruff, S. W., et al. (2013). Geochemical consequences of widespread clay mineral formation in Mars' ancient crust. *Space Science Reviews*, *174*, 329–364. https://doi.org/10.1007/s11214-012-9930-0
Eugster, H. P. (1980). Geochemistry of evaporitic lacustrine deposits. *Annual Review of Earth and Planetary Sciences*, *8*(1), 35–63. https://doi.org/10.1146/annurev.ea.08.050180.000343
Fassett, C. I., & Head, J. W. (2007). Layered mantling deposits in northeast Arabia Terra, Mars: Noachian-Hesperian sedimentation, erosion, and terrain inversion. *Journal of Geophysical Research*, *112*(8), E08002. https://doi.org/10.1029/2006JE002875
Gaillard, F., Michalski, J., Berger, G., McLennan, S. M., & Scaillet, B. (2013). Geochemical reservoirs and timing of sulfur cycling on Mars. *Space Science Reviews*, *174*(1–4), 251–300. https://doi.org/10.1007/s11214-012-9947-4
Gillmann, C., Lognonné, P., & Moreira, M. (2011). Volatiles in the atmosphere of Mars: The effects of volcanism and escape constrained by isotopic data. *Earth and Planetary Science Letters*, *303*(3–4), 299–309. https://doi.org/10.1016/j.epsl.2011.01.009
Glaze, L. S., & Baloga, S. M. (2002). Volcanic plume heights on Mars: Limits of validity for convective models. *Journal of Geophysical Research*, *107*(E10), 5086. https://doi.org/10.1029/2001JE001830
Golombek, M. P., Grant, J. A., Crumpler, L. S., Greeley, R., Arvidson, R. E., Bell, J. F., et al. (2006). Erosion rates at the Mars Exploration Rover landing sites and long-term climate change on Mars. *Journal of Geophysical Research*, *111*(12), E12S10. https://doi.org/10.1029/2006JE002754
Greeley, R. (1987). Release of juvenile water on Mars: Estimated amounts and timing associated with volcanism. *Science*, *236*(4809), 1653–1654. https://doi.org/10.1126/science.236.4809.1653
Greeley, R., & Crown, D. A. (1990). Volcanic geology of Tyrrhena Patera, Mars. *Journal of Geophysical Research*, *95*(B5), 7133–7149. https://doi.org/10.1029/JB095iB05p07133
Greeley, R., & Schneid, B. D. (1991). Magma generation on Mars: Amounts, rates, and comparisons with Earth, moon, and venus. *Science*, *254*(5034), 996–998. https://doi.org/10.1126/science.254.5034.996
Greeley, R., & Spudis, P. D. (1981). Volcanism on Mars. *Reviews of Geophysics*, *19*, 13. https://doi.org/10.1029/RG019i001p00013
Gross, L. C., Carter, J., Poulet, F., Loizeau, D., Bishop, J. L., Horgan, B., & Michalski, J. (2017). Mawrth vallis – an auspicious destination for the ESA and NASA 2020. In *Lunar and Planetary Science* (Vol. XLVIII, p. 2194). Retrieved from https://www.hou.usra.edu/meetings/lpsc2017/pdf/2194.pdf
Hewett, D., & Lupton, C. (1917). *Anticlines in the Southern Part of the Big Horn Basin, Wyoming: A Preliminary Report on the Occurrence of Oil*. (Vol. 656). U.S. Geological Survey Bulletin.
Hodges, C. A., & Moore, H. J. (1994). Atlas of volcanic landforms on Mars. (Vol. 1534, pp. 424–452). *US Geological Survey Professional Paper*. https://doi.org/10.3133/pp1534
Horvath, D. G., Moitra, P., Hamilton, C. W., Craddock, R. A., & Andrews-Hanna, J. C. (2021). Evidence for geologically recent explosive volcanism in Elysium Planitia, Mars. *Icarus*, (Vol. 365, p. 114499). Academic Press. https://doi.org/10.1016/J.ICARUS.2021.114499
Hynek, B. M., Phillips, R. J., & Arvidson, R. E. (2003). Explosive volcanism in the Tharsis region: Global evidence in the Martian geologic record. *Journal of Geophysical Research*, *108*(E9), 5111. https://doi.org/10.1029/2003JE002062
Isherwood, R. J., Jozwiak, L. M., Jansen, J. C., & Andrews-Hanna, J. C. (2013). The volcanic history of Olympus Mons from paleo-topography and flexural modeling. *Earth and Planetary Science Letters*, *363*, 88–96. https://doi.org/10.1016/j.epsl.2012.12.020
Keller, W. D. (1970). Environmental aspects of clay minerals. *SEPM Journal of Sedimentary Research*, *40*, 155–161 https://doi.org/10.1306/74d720a4-2b21-11d7-8648000102c1865d
Kerber, L., Forget, F., Madeleine, J. B., Wordsworth, R., Head, J. W., & Wilson, L. (2013). The effect of atmospheric pressure on the dispersal of pyroclasts from martian volcanoes. *Icarus*, *223*(1), 149–156. https://doi.org/10.1016/j.icarus.2012.11.037
Kerber, L., Head, J. W., Madeleine, J. B., Forget, F., & Wilson, L. (2011). The dispersal of pyroclasts from Apollinaris Patera, Mars: Implications for the origin of the Medusae Fossae Formation. *Icarus*, *216*(1), 212–220. https://doi.org/10.1016/j.icarus.2011.07.035
Kerber, L., Head, J. W., Madeleine, J. B., Forget, F., & Wilson, L. (2012). The dispersal of pyroclasts from Apollinaris Patera, Mars: Implications for the friable layered deposits. *Icarus*, *219*(1), 358–381. https://doi.org/10.1016/2012.03.1610.1016/j.icarus.2012.03.016
Kerber, L., Michalski, J. R., Bleacher, J. E., & Forget, F. (2013). *Ash Sources? Implication for the Arabia Deposits. Lunar & Planetary Science Conference, 2290*.
Lammer, H., Chassefière, E., Karatekin, Ö., Morschhauser, A., Niles, P. B., Mousis, O., et al. (2013). Outgassing history and escape of the martian atmosphere and water inventory. *Space Science Reviews*, *174*(1–4), 113–154. https://doi.org/10.1007/s11214-012-9943-8
Liu, J., Michalski, J. R., Tan, W., He, H., Ye, B., & Xiao, L. (2021). Anoxic chemical weathering under a reducing greenhouse on early Mars. *Nature Astronomy*, *5*, 503–509. https://doi.org/10.1038/s41550-021-0110.1038/s41550-021-01303-5
Lockwood, J. P., & Lipman, P. W. (1987). Holocene eruptive history of Mauna Loa Volcano. *U. S. Geological Survey Professional Paper*, *1350*, 509–535
Lowe, R. L., Bishop, J. L., Loizeau, D., Wray, J. J., & Beyer, R. A. (2020). Deposition of >3.7 Ga clay-rich strata Mawrth Vallis Group, Mars in lacustrine, alluvial and aeolian environments. *GSA Bulletin*, (Vol. 132, pp. 17–30). https://doi.org/10.1130/B35185.1

Malin, M. C., Bell, J. F., Cantor, B. A., Caplinger, M. A., Calvin, W. M., Clancy, R. T., et al. (2007). Context camera investigation on board the Mars Reconnaissance Orbiter. *Journal of Geophysical Research*, *112*(E5), E05S04. https://doi.org/10.1029/2006je002808

Matthews, N., Smith, V., Costa, A., & Durant, A. (2011). Ultra-distal Tephra Deposits from Supereruptions: Examples from Toba and New Zealand. November 2015. *Quaternary International*, *258*, 54–79. https://doi.org/10.1016/j.quaint.2011.07.010

McEwen, A. S., Eliason, E. M., Bergstrom, J. W., Bridges, N. T., Hansen, C. J., Delamere, W. A., et al. (2007). Mars reconnaissance orbiter's high resolution imaging science experiment (HiRISE). *Journal of Geophysical Research*, *112*(E5), E05S02. https://doi.org/10.1029/2005je002605

McGill, G. E. (2000). Crustal history of north central Arabia Terra, Mars. *Journal of Geophysical Research*, *105*, 6945–6959. https://doi.org/10.1029/1999JE001175

McKeown, N. K., Noe Dobrea, E. Z., Bishop, J. L., & Silver, E. A. (2009). Coordinated lab, field, and aerial study of the Painted Desert, AZ, as a potential analog site for phyllosilicates at Mawrth Vallis, Mars. In *Lunar and Planetary Science Conference XL*. Retrieved from https://ui.adsabs.harvard.edu/abs/2009LPI.40.2509M/abstract

Michalski, J. R., & Bleacher, J. E. (2013). Supervolcanoes within an ancient volcanic province in Arabia Terra, Mars. *Nature*, *502*(7469), 47–52. https://doi.org/10.1038/nature12482

Milliken, R. E., Swayze, G. A., Arvidson, R. E., Bishop, J. L., Clark, R. N., Ehlmann, B. L., et al. (2008). Opaline silica in young deposits on Mars. *Geology*, *36*(11), 847–850. https://doi.org/10.1130/G24967A.1

Moore, J. M. (1990). Nature of the mantling deposit in the heavily cratered terrain of northeastern Arabia, Mars. *Journal of Geophysical Research*, *95*(B9), 14279. https://doi.org/10.1029/JB095iB09p14279

Moratto, S. Z. M., Broxton, M. J., Beyer, R., Lundy, M., & Husmann, K. (2010). Ames Stereo Pipeline , NASA ' s Open Source Automated Stereogrammetry. In *41st Lunar and Planetary Science Conference*. (Vol. 41, pp. 1–2).

Murchie, S., Arvidson, S., Bedini, P., Beisser, K., Bibring, J.-P., Bishop, J., et al. (2007). Compact reconnaissance imaging spectrometer for Mars (CRISM) on Mars reconnaissance orbiter (MRO). *Journal of Geophysical Research*, *112*, E05S03. https://doi.org/10.1029/2006JE002682

Newhall, C., & Self, S. (1982). The Volcanic Explosivity Index (VEI) an estimate of explosive magnitude for historical volcanism. *Journal of Geophysical Research*, *87*(C2), 1231–1238. https://doi.org/10.1029/jc087ic02p01231

Osinski, G. R. (2005). Hydrothermal activity associated with the Ries impact event, Germany. *Geofluids*, *5*, 202–220. https://doi.org/10.1111/j.1468-8123.2005.00119.x

Perrin, S. L., Bishop, J. L., Sessa, A. M., Perrin, S. L., Bishop, J. L., & Sessa, A. M. (2019). Analysis of Unique Martian Sulphate Outcrops Based on Samples from the Painted Desert Sulphate Hill Analog Site and Lab Mixtures. *LPI*. (p. 1903). Retrieved from https://ui.adsabs.harvard.edu/abs/2019LPI.50.1903P/abstract

Phillips, R. J., Zuber, M. T., Solomon, S., Glombek, M. P., Jakosky, B. M., Banerdt, W. B., et al. (2001). Ancient geodynamics and global-scale hydrology on Mars. *Science*, *291*(5513), 2587–2591. https://doi.org/10.1126/science.1058701

Platz, T., Michael, G., Tanaka, K. L., Skinner, J. A., & Fortezzo, C. M. (2013). Crater-based dating of geological units on Mars: Methods and application for the new global geological map. *Icarus*, *225*(1), 806–827. https://doi.org/10.1016/J.ICARUS.2013.04.021

Plescia, J. B., & Crisp, J. (1992). Recent Elysium volcanism; effects on the Martian atmosphere. In *Workshop on the Martian Surface and Atmosphere through Time*. (Vol. 92–2, pp. 115–116)

Rampe, E. B., Kraft, M. D., Sharp, T. G., Ming, D. W., Golden, C., & Christensen, P. R. (2012). Allophane detection on Mars with Thermal Emission Spectrometer data and implications for regional-scale chemical weathering processes. *Geology*, *40*, 995–998. https://doi.org/10.1130/g33215.1

Richardson, J., Bleacher, J., Connor, C., & Glaze, L. (2021). Small volcanic vents of the Tharsis Volcanic Province, Mars. *Journal of Geophysical Research: Planets*, *126*. https://doi.org/10.1029/2020JE006620

Richardson, J. A., Whelley, P. L., & Matiella, M. A. (2021). *Elevation dataset for: Stratigraphic evidence for early martian explosive volcanism in Arabia Terra*. Digital Repository at the University of Maryland. https://doi.org/10.13016/bez2-agt8. Retrieved from https://drum.lib.umd.edu/handle/1903/27174

Rooyakkers, S. M., Stix, J., Berlo, K., & Barker, S. J. (2020). Emplacement of unusual rhyolitic to basaltic ignimbrites during collapse of a basalt-dominated caldera: The Halarauður eruption, Krafla (Iceland). *GSA Bulletin*, *132*(9–10), 1881–1902. https://doi.org/10.1130/B35450.1

Ross, C. S., & Shannon, E. V. (1926). The minerals of bentonite and related clays and their physical properties1. *Journal of the American Ceramic Society*, *9*(2), 77–96. https://doi.org/10.1111/j.1151-2916.1926.tb18305.x

Ruff, S. W. W., & Christensen, P. R. (2002). Bright and dark regions on Mars: Particle size and mineralogical characteristics based on Thermal Emission Spectrometer data. *Journal of Geophysical Research*, *E12*(107), 5127. https://doi.org/10.1029/2001je001580. Retrieved from http://www.mars.asu.edu/~ruff/DCI/2001JE001580.pdf

Schiffman, P., Zierenberg, R., Marks, N., Bishop, J. L., & Darby Dyar, M. (2006). Acid-fog deposition of Kilauea volcano: A possible mechanism for the formation of siliceous-sulphate rock coatings on Mars. *Geology*, *34*(11), 921–924. https://doi.org/10.1130/G22620A.1

Seelos, F. P., Morgan, M. F., TaylorMurchie, H. S. L., Humm, D. C., Seelos, K. D., et al. (2012). CRISM Map Projected Targeted Reduced Data Records (MTRDRs)–High level analysis and visualization data products. In L. Gaddis, T. Hare, & R. Beyer (Eds.), Summary and abstracts of the planetary data workshop, june 2012, U.S (Vol. 1056, p. 199). Geological Survey Open-File Report 2014–1056. https://doi.org/10.3133/ofr20141056

Seelos, K. D., Arvidson, R. E., Jolliff, B. L., Chemtob, S. M., Morris, R. V., Ming, D. W., & Swayze, G. A. (2010). Silica in a Mars analog environment: Ka u Desert, Kilauea Volcano, Hawaii. *Journal of Geophysical Research*, *115*(4), E00D15. https://doi.org/10.1029/2009JE003347

Sharp, R. P. (1973). Mars: Fretted and chaotic terrains. *Journal of Geophysical Research*, *78*(20), 4073–4083. https://doi.org/10.1029/JB078i020p04073

Sheppard, R. A., & Hay, R. L. (2001). Formation of zeolites in open hydrologic systems. *Reviews in Mineralogy and Geochemistry*, *45*, 261–275. https://doi.org/10.2138/rmg.2001.45.8

Sherman, G. D., & Uehara, G. (1956). The weathering of Olivine Basalt in Hawaii and its pedogenic significance. *Soil Science Society of America Journal*, *20*, 337–340. https://doi.org/10.2136/sssaj1956.03615995002000030011x

Smith, D. E., Zuber, M. T., Frey, H. V., Garvin, J. B., Head, J. W., Muhleman, D. O., et al. (2001). Mars orbiter laser altimeter: Experiment summary after the first year of global mapping of Mars. *Journal of Geophysical Research*, *106*(E10), 23689–23722. https://doi.org/10.1029/2000JE001364

Svenson, M. J. O., Osinski, G. R., Caudill, C. M., Goudge, T. A., Longstaffe, F. J., Sapers, H. M., & Tornabene, L. T. (2021). The Ries Impact Structure, Germany: Insight into the Role of Impact Cratering in Forming Clay Minerals on Mars. *Terrestrial Analogs. (LPI Contribution No. 2595)*. (Vol. 2021).

Tanaka, K. L. (2000). Dust and ice deposition in the Martian geologic record. *Icarus*, *144*(2), 254–266. https://doi.org/10.1006/icar.1999.6297

Viviano-Beck, C. E., Murchie, S. L., Beck, A. W., & Dohm, J. M. (2017). Compositional and structural constraints on the geologic history of eastern Tharsis Rise, Mars. *Icarus*, *284*, 43–58. https://doi.org/10.1016/j.icarus.2016.09.005

Viviano-Beck, C. E., Seelos, F. P., Murchie, S. L., Kahn, E. G., Seelos, K. D., Taylor, H. W., et al. (2014). Revised CRISM spectral parameters and summary products based on the currently detected mineral diversity on Mars. *Journal of Geophysical Research: Planets*, *119*(6), 1403–1431. https://doi.org/10.1002/2014je004627

Weisenberger, T., & Selbekk, R. S. (2009). Multi-stage zeolite facies mineralization in the Hvalfjrdur area, Iceland. *International Journal of Earth Sciences*, *98*(5), 985–999. https://doi.org/10.1007/s00531-007-0296-6

Whelley, P. L., Newhall, C. G., & Bradley, K. E. (2015). The frequency of explosive volcanic eruptions in Southeast Asia. *Bulletin of Volcanology*, *77*(1), 1–35. https://doi.org/10.1007/s00445-014-0893-8

Wherry, E. T. (1917). Clay derived from volcanic dust in the Pierre of South Dakota. *Journal of the Washington Academy of Sciences*, *7*, 576–583. https://doi.org/10.2307/1543949. Retrieved from https://www.jstor.org/stable/24521366

Wicks, C. W., Thatcher, W., Dzurisin, D., & Svarc, J. (2006). Uplift, thermal unrest and magma intrusion at Yellowstone caldera. *Nature*, *440*(7080), 72–75. https://doi.org/10.1038/nature04507

Williams, D., Greeley, R., Fergason, R. L., Kuzmin, R., McCord, T. B., Combe, J.-P., et al. (2009). The Circum-Hellas Volcanic Province, Mars: Overview. *Planetary & Space Science*, *57*(8–9), 895–916. https://doi.org/10.1016/j.pss.2008.08.010

Wilson, L., & Head, J. W. (2007). Explosive volcanic eruptions on Mars: Tephra and accretionary lapilli formation, dispersal and recognition in the geologic record. *Journal of Volcanology and Geothermal Research*, *163*, 83–97. https://doi.org/10.1016/j.jvolgeores.2007.03.007

Xiao, L., Huang, J., Christensen, P. R., Greeley, R., Williams, D. A., Zhao, J., & He, Q. (2012). Ancient volcanism and its implication for thermal evolution of Mars. *Earth and Planetary Science Letters*, *323–324*, 9–18. https://doi.org/10.1016/j.epsl.2012.01.027

Ye, B., & Michalski, J. R. (2021). Precipitation-driven pedogenic weathering of volcaniclastics on early Mars. *Geophysical Research Letters*, *48*, e2020GL091551. https://doi.org/10.1029/2006JE00275610.1029/2020gl091551

Zuber, M. T. (2001). The crust and mantle of Mars. *Nature*, *412*, 220–227. https://doi.org/10.1038/35084163